AGU PUBLICATIONS

Geophysical Research Letters

RESEARCH LETTER
10.1002/2016GL071016

Key Points:
- A new dust emission scheme that includes soil water and dynamic vegetation greatly increases long-term variability of Australian dust
- Using the new parameterization CM3 gains the ability to simulate the observed ENSO-dust relationship over Australia
- Increased dust variability has large impacts on the surface energy balance and possibly precipitation

Correspondence to:
S. Evans,
smevans@princeton.edu

Citation:
Evans, S., P. Ginoux, S. Malyshev, and E. Shevliakova (2016), Climate-vegetation interaction and amplification of Australian dust variability, *Geophys. Res. Lett.*, *43*, 11,823–11,830, doi:10.1002/2016GL071016.

Received 26 AUG 2016
Accepted 3 NOV 2016
Accepted article online 5 NOV 2016
Published online 23 NOV 2016

Climate-vegetation interaction and amplification of Australian dust variability

Stuart Evans[1], Paul Ginoux[2], Sergey Malyshev[3], and Elena Shevliakova[1,2]

[1]Princeton Environmental Institute, Princeton University, Princeton, New Jersey, USA, [2]NOAA/Geophysical Fluid Dynamics Laboratory, Princeton, New Jersey, USA, [3]Deparment of Ecology and Evolutionary Biology, Princeton University, Princeton, New Jersey, USA

Abstract Observations show that Australian dust activity varies by a factor of 4 on decadal timescales. General circulation models, however, typically fail to simulate this variability. Here we introduce a new dust parameterization into the NOAA/Geophysical Fluid Dynamics Laboratory climate model CM3 that represents land surface processes controlling dust sources including soil water and ice, snow cover, vegetation characteristics, and land type. In an additional novel step, we couple this new dust parameterization to the dynamic vegetation model LM3. In Australia, the new parameterization amplifies the magnitude and timescale of dust variability and better simulates the El Niño–Southern Oscillation-dust relationship by more than doubling its strength. We attribute these improvements primarily to the slow response time of vegetation to precipitation anomalies and show that vegetation changes account for approximately 50% of enhanced dust emission during El Niño events. The amplified dust leads to radiative forcing over Australia greater than −1 and −20 W/m^2 at top of atmosphere and surface, respectively.

1. Introduction

Dust is a strong driver of regional climate near and downwind from source regions [*Shao et al.*, 2011]. Scattering and absorption of radiation by dust in the atmospheric column impacts surface energy fluxes and the stability of the atmosphere, and deposition of dust from the atmosphere to the ocean is important to biogeochemical cycles. In Australia, the Lake Eyre basin (centered at 28.4°S, 137.4°E) is the largest dust source [*Ginoux et al.*, 2012; *Prospero et al.*, 2002]. Dust from Lake Eyre and its surrounding basin has been shown to impact precipitation [*Rotstayn et al.*, 2011] and air quality [*Chan et al.*, 2005; *Leys et al.*, 2011] in Australia, while farther downwind it is important to the productivity of the Tasman Sea and Southern Ocean [*Boyd et al.*, 2004; *Gabric et al.*, 2010], and its accumulation is used as a paleoclimate proxy in New Zealand [*Marx et al.*, 2009] and Antarctica [*Revel-Rolland et al.*, 2006].

Observations show that the occurrence and intensity of dust from Australia has substantial variability at seasonal, interannual, and decadal timescales [*Strong et al.*, 2010; *Leys et al.*, 2008; *Goudie and Middleton*, 1992]. General circulation models (GCMs), however, typically struggle to reproduce this variability, particularly at interannual and longer timescales [*Evan et al.*, 2014]. In some cases, high dust variability has been achieved by constraining the strength of different source regions with observations [*Mahowald et al.*, 2010], but to the best of our knowledge, it has not been accomplished in an unconstrained model. One commonly suggested reason for this lack of variability in models is the inability to simulate the effects of land surface changes on dust emission [*Stanelle et al.*, 2014; *Zender and Kwon*, 2005]. When land surface changes have been prescribed in GCMs [e.g., *Cook et al.*, 2009], amplified changes in dust emission have been the result. In this study, we show that incorporating land surface information into the dust emission parameterization produces much more realistic long timescale variability, without prescribing changes to the land surface or source strength.

Dust emission from the Lake Eyre basin peaks in austral summer (December-January-February, DJF) [*Prospero et al.*, 2002; *Strong et al.*, 2010]. Summer rainfall and drought in this region are most strongly tied to the El Niño–Southern Oscillation (ENSO) [*Risbey et al.*, 2009], which reduces rainfall in El Niño years. The range of rainfall that central Australia experiences is great enough that Lake Eyre can be completely dry for years at a time and deep enough at other times to support the existence of the Lake Eyre Yacht Club. These fluctuations in water availability naturally bring fluctuations in vegetation cover as well [*Lotsch et al.*, 2003]. Other drivers of Australian rainfall are less important there, though there are potential indirect effects. The Australian monsoon does not reach as far south as Lake Eyre [*Wang and Ding*, 2008], though it does

contribute to rainfall in the northernmost catchments of the Lake Eyre drainage basin. The monsoon is shorter and less active in El Niño years [*Evans et al.*, 2014], meaning that the influence it has on Lake Eyre water levels is in concert with local precipitation variability. The Indian Ocean Dipole is also important to precipitation in Australia, though it is most strongly connected to variability in western and southern Australia and during the June-July-August and September-October-November seasons [*Risbey et al.*, 2009]. These seasons contribute less than DJF to both the total precipitation and the precipitation variability in central Australia, making the Indian Ocean Dipole less important than ENSO for summertime soil water and vegetation. Collectively, the high range of rainfall and limited number of drivers of that rainfall make central Australia an ideal testbed for the importance of the land surface to dust emission.

2. Experimental Design

For our study, we use the NOAA/GFDL (Geophysical Fluid Dynamics Laboratory) coupled GCM CM3 [*Donner et al.*, 2011] which includes the dynamic land model LM3 [*Shevliakova et al.*, 2009; *Milly et al.*, 2014]. For computational efficiency we use a version of CM3 with simplified atmospheric chemistry. The standard version of CM3 calculates dust emission into the lowest layer of the atmosphere according to *Ginoux et al.* [2001],

$$\text{emission} = C_H \cdot \text{frac}_{\text{land}} \cdot \text{source} \cdot {u_{10\text{m}}}^2 \cdot (u_{10\text{m}} - u_{\text{thresh}}) \quad (1)$$

where $u_{10\text{m}}$ is the 10 m wind speed, u_{thresh} is the minimum wind speed for dust emission, $\text{frac}_{\text{land}}$ is the fraction of the grid cell that is land, C_H is a scaling constant, and source is a temporally invariant source map that preferentially emits dust from topographic depressions with bare soil. Locations with bare soil are estimated from satellite data from the year 2000. Notably, the only temporally varying variable in equation (1) is 10 m wind speed. Emitted dust is partitioned into five size bins (0.1–1 μm, 1–2 μm, 2–3 μm, 3–6 μm, and 6–10 μm radius) with each bin receiving a fixed percentage of the total emitted mass (10% for the smallest size bin and 22.5% each for the other four). Once in the atmosphere, the dust tracers corresponding to each bin are transported by advection, vertical diffusion, and gravitational settling. While in the atmosphere dust both absorbs and scatters radiation, with radiative properties determined by *Balkanski et al.* [2007] for shortwave and *Volz* [1973] for longwave. Dust in CM3 is not chemically active, nor does it interact with cloud microphysics. Removal of dust is accounted for by three mechanisms: gravitational settling, dry deposition at the surface from turbulence, and wet deposition from both in-cloud scavenging and below-cloud scavenging.

The new dust emission parameterization maintains dependencies on wind speed and topography and also incorporates information regarding soil water and ice, snow cover, vegetation coverage, and land type. LM3 describes the land within each grid cell as a collection of tiles of various types, categorized as either natural, secondary (previously harvested or used for agriculture), pasture, croplands, lake, or glacier. Each tile in a grid cell experiences the same forcing from the atmosphere above but responds with its own vegetation, soil properties, and surface fluxes. Dust emission is calculated separately for each land tile to account for differences in surface properties and then aggregated and passed to lowest layer of the atmosphere. The new dust emission equation is

$$\text{emission} = C_H \cdot F(\text{moisture}) \cdot \text{bareness} \cdot \text{source} \cdot {u_{\text{fric}}}^2 \cdot (u_{\text{fric}} - u_{\text{thresh}}) \quad (2)$$

Land type directly affects dust emission through u_{thresh}, which varies by tile type, being larger for pasture and croplands than for natural and secondary vegetation and infinite for lakes and glaciers. F(moisture) incorporates threshold values of soil water and ice, and snow cover, above which dust emission becomes zero. Vegetation influence is accounted for by using leaf area index (LAI) and stem area index (SAI) to calculate a bareness fraction for each land tile. Bareness equals 1 when LAI and SAI are both zero and exponentially decays as LAI and SAI increase. Thus, as vegetation LAI and SAI increase, bareness decreases, and dust emission decreases linearly with bareness. Vegetation in LM3 can either be prescribed as a static cycle or be simulated dynamically to be responsive to variations in weather and climate in the experiment. The final difference between the emission schemes is that 10 m wind speed is replaced with the surface friction velocity, a more accurate measure of the wind's ability to mobilize dust. For friction velocity the wind speed thresholds are 0.8 m/s for pasture and croplands and 0.25 m/s for natural and secondary vegetation. These values are broadly in keeping with those estimated by *Shao and Leslie* [1997] for dust emission from central Australia. Once in the atmosphere, dust is treated exactly as in the standard configuration of CM3.

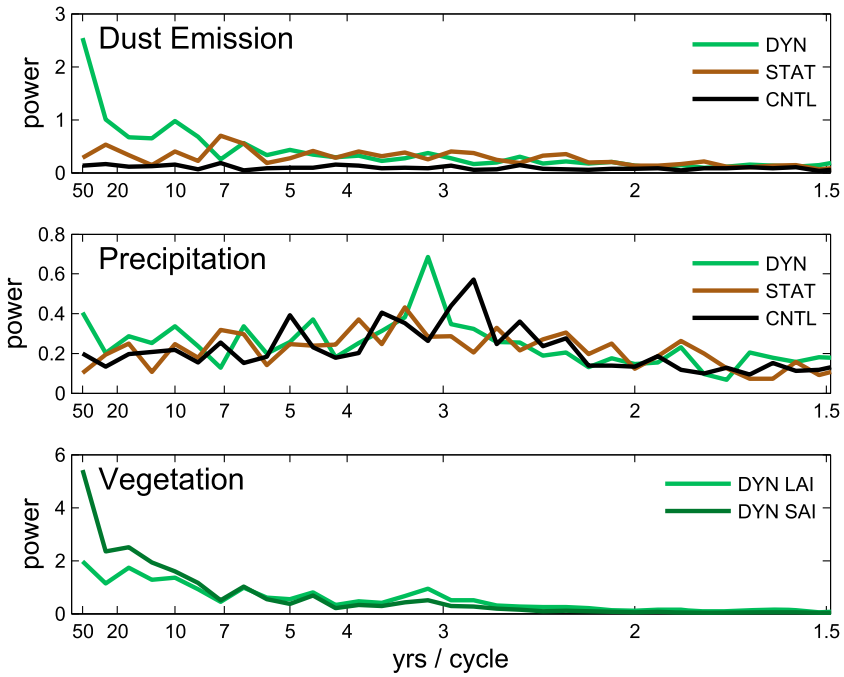

Figure 1. Power spectra for (top) dust emission, (middle) precipitation, and (bottom) vegetation indices for central Australia (20–40°S, 130–145°E). Green lines represent the DYN experiment, brown lines the STAT experiment, and black lines the CNTL experiment. Spectra are calculated after the seasonal cycle is removed and are the average of spectra from ten 50 year chunks of the model time series.

Using the two different parameterizations of dust emission in CM3, we investigate the internal variability of dust in three 500 year preindustrial experiments. All experiments are performed at approximately $2° \times 2°$ resolution using constant 1860 forcings and CMIP5 land-type distributions [*Hurtt et al.*, 2011]. In Australia, the preindustrial land type is entirely natural or lake, meaning that there is no anthropogenic dust from pasture or croplands. The experiments differ in two respects: dust emission parameterization and vegetation. The control experiment (CNTL) uses the standard emission parameterization (equation (1)) that does not account for the influence of vegetation or soil moisture and has prescribed vegetation in a static annual cycle. The second experiment (STAT) uses the same static vegetation loop as the control run but the new dust emission parameterization (equation (2)). The third experiment (DYN) uses both the new dust emission parameterization and dynamic vegetation. The DYN vegetation is initialized from the static vegetation state and then allowed to respond to the weather and climate that it experiences.

3. Results

To evaluate the dust variability produced by the new parameterization, we begin by examining the power spectra of monthly mean dust emission from central Australia, defined as land between 20–40°S and 130–145°E, in the three experiments. Figure 1 (top) shows the increase in low-frequency power most obviously for the DYN experiment at decadal timescales, but also in the STAT experiment, and at interannual timescales. At timescales of approximately 2–7 years, both the DYN and STAT experiments show an increase in spectral power. This is primarily the effect of dust emission responding to changes in soil moisture on those timescales. Figure 1 (middle) shows the power spectra of monthly mean precipitation for the same region, with a peak for all experiments at interannual timescales, which we attribute to the approximately 3 year spectral peak of ENSO in the model. While all three experiments have similar ENSO-related precipitation variability at the same timescales, dust emission only responds in the DYN and STAT experiments because only the new emission parameterization is responsive to changes in soil moisture due to changes in rainfall. The peak in spectral power at interdecadal timescales in the DYN experiment is a direct result of dust emission responding to variability in vegetation characteristics at similar timescales, shown in Figure 1 (bottom).

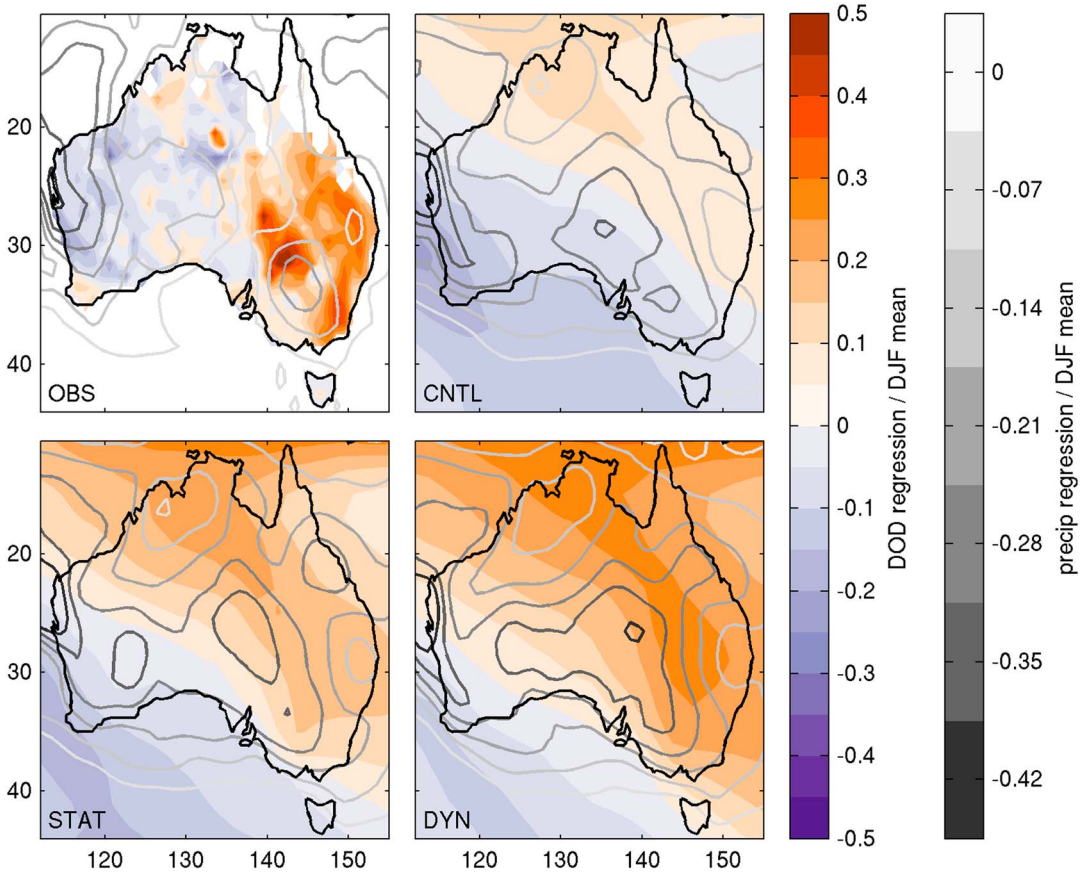

Figure 2. Regional patterns of dust optical depth (DOD) and precipitation responses to ENSO in observations and the three model runs. (top left) Observations (MODIS Deep Blue 2003–2015 and GPCP 1979–2015), (top right) the control run, (bottom left) static vegetation, and (bottom right) dynamic vegetation. Shading (intervals of 0.05) indicates changes in DOD, and grey contours (intervals of 0.07) indicate changes in precipitation. Values are the regression coefficient between DJF-averaged DOD (precipitation) and the DJF Nino3.4 index divided by the DJF mean DOD (precipitation). Thus, a value of 0.5 indicates a 50% increase per unit Nino3.4 during DJF. Positive Nino3.4 values indicate El Niño conditions.

When allowed to respond to varying weather and climate, plants in the model grow and die relatively slowly compared to meteorological anomalies. Effectively, the plants, particularly their stems that are used to calculate SAI, integrate weather over multiple years and then imprint that information on dust emission.

Having shown that the new dust source parameterization increases the low-frequency variability previously lacking in CM3, we also demonstrate that the mechanisms giving rise to such increased variability do so for the right reasons. As ENSO is clearly a major driver of variability in Australia on interannual timescales, we now examine the ENSO-dust relationship as a test of the dust emission processes. We use December-January-February (DJF) seasonal means for this, when both ENSO events and Australian dust emission typically peak. Figure 2 shows the spatial relationships between dust optical depth (DOD), precipitation, and ENSO in satellite retrievals and the three experiments. Each panel shows the fractional change in seasonal DOD and precipitation (defined as the regression coefficient divided by the seasonal mean) per unit of the Nino3.4 index. For observations, DOD is derived from Moderate Resolution Imaging Spectroradiometer (MODIS) Collection 6 Deep Blue aerosol optical depth [*Sayer et al.*, 2013; *Hsu et al.*, 2013] 2003–2015 data using the relationship established by *Anderson et al.* [2005] from in situ data. The precipitation data are Global Precipitation Climatology Project (GPCP) monthly means [*Adler et al.*, 2003; *Huffman et al.*, 2009] spanning 1979–2015. As can be seen in the observations, during El Niño years (i.e., positive Nino3.4), rainfall decreases over Australia, particularly in the southeast, and DOD increases, by as much as 50% over sources in the Lake Eyre region. DOD also shows strong increases in eastern and southeastern Australia, where anthropogenic land use contributes to dust emission [*Ginoux et al.*, 2012].

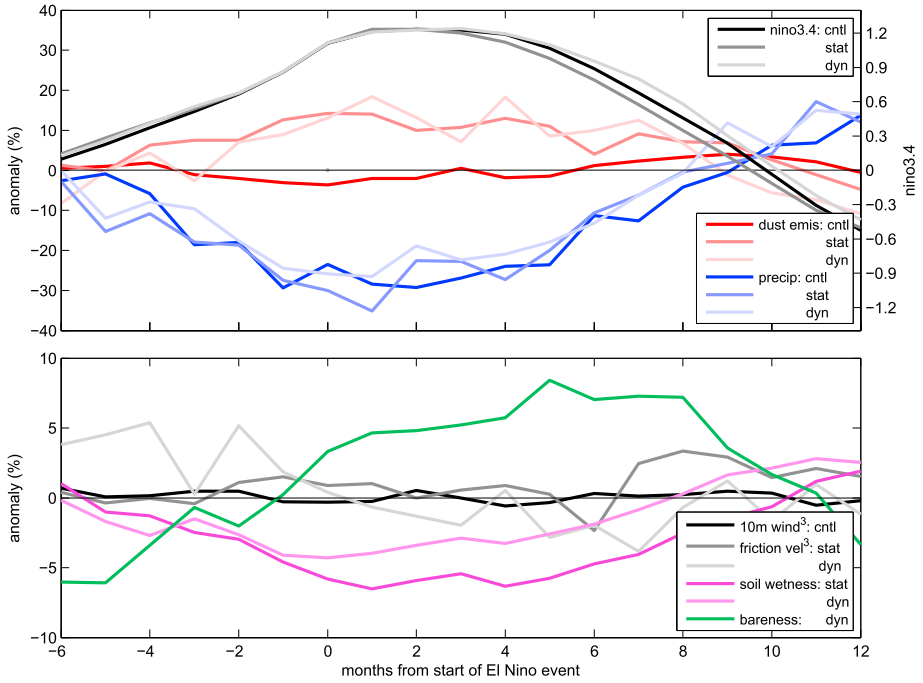

Figure 3. Composite evolution of central Australian (20–40°S, 130–145°E) dust emission and related variables during El Niño events. Events are composited from 6 months before to 12 months after the Nino3.4 index first exceeds a value of 1. Curves represent 148 events for CNTL, 152 events for STAT, and 147 events for DYN. (top) Black/grey lines show the evolution of the Nino3.4 index (right axis). All other curves show the percent anomaly from the climatological seasonal cycle, i.e., $100*(x_i - \overline{x})/\overline{x}$ (left axes). As an example, the blue curves of Figure 3 (top) indicate that at the start of an El Niño event, precipitation in central Australia is ~25–30% less than normal. Families of curves, indicated by color, represent the same variable plotted from different model runs. (bottom) The black/grey curves in represent the appropriate wind variable used in the dust emission equation—10 m wind speed for CNTL and friction velocity for STAT and DYN.

The CNTL experiment produces an ENSO-precipitation relationship for the region that is somewhat stronger than observations but still fails almost entirely to simulate the observed ENSO-DOD relationship. Without knowledge of the ENSO-induced drying, the original dust emission scheme has no mechanism to increase dust production in this simulation. In this case, the modest (<10%) increase in DOD over northern and eastern Australia comes not from increased dust emission (as can be seen in Figure 3) but rather from decreased wet scavenging due to reduced precipitation (not shown). The STAT experiment has a slightly stronger precipitation anomaly than CNTL, but in this experiment dust emission responds to variations of soil moisture, approximately doubling the dust response of the CNTL experiment. While much improved, this still falls short of the observed strength of the relationship between ENSO and DOD. The DYN experiment has a moderately greater precipitation response, with dust emission responding not only to soil drying but also to the consequent vegetation dieback. The result is a DOD response (~25%) that comes close to matching the strength of the observed relationship, though not the peak values directly over the sources. One possible reason that the model still does not quite equal the strength of the observed relationship is the model's inability to represent the shrinking of Lake Eyre that happens during droughts, due to both local evaporation and reduced rainfall in all parts of the catchment basin.

To illuminate the processes that contribute to the three experiments' varying ability to reproduce the observed ENSO-dust relationship, we show the evolution of dust and related variables for El Niño events in Figure 3. We define El Niño events as beginning each time the Nino3.4 index increases to a value greater than 1. This definition produces approximately 150 events in each experiment. We composite monthly mean values of a set of dust-relevant variables from 6 months before to 12 months after the event start time in order to show evolution over the entire event. As shown in Figure 3 (top), the Nino3.4 index evolves similarly in all three experiments, with approximately the same shape, duration, and magnitude. Additionally, the precipitation anomalies that central Australia experiences are approximately the same between experiments.

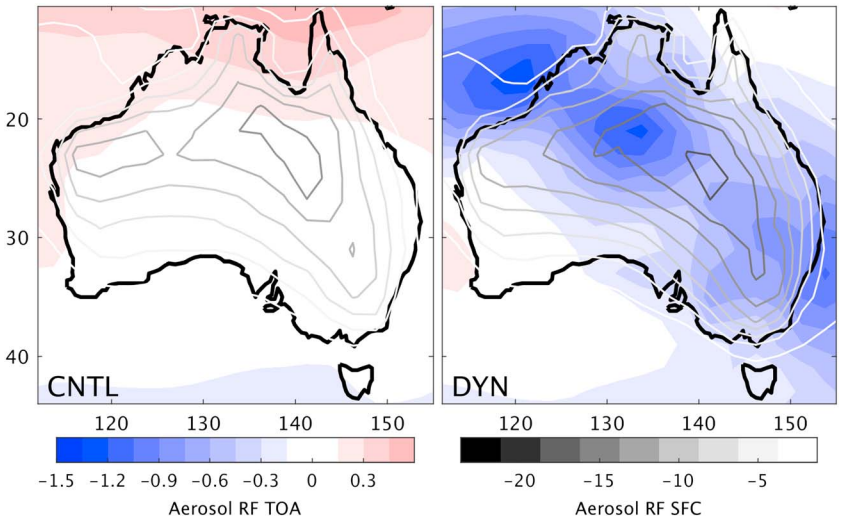

Figure 4. Spatial distribution of regression coefficients (W/m^2/Nino3.4) for clear-sky aerosol radiative forcing at TOA (shading, left color bar, intervals of 0.15) and the surface (contours, right color bar, intervals of 2.5) in (left) the CNTL experiment and (right) the DYN experiment.

Thus, differences in the Australian dust response to El Niño events are due to neither differences in ENSO nor the local precipitation response to ENSO. Despite these similarities, we see that the STAT and DYN experiments experience a ~10–15% increase in dust emission for several months after the beginning of the El Niño, while the CNTL experiment shows no change. To explain this difference, we investigate the variables that directly affect dust emission in the two parameterizations.

Figure 3 (bottom) shows the composite anomalies associated with El Niño events for the three time-varying variables—surface wind, soil wetness, and bareness—that are part of equations (1) and (2). We use the surface wind variable used in each experiment's dust emission calculation (10 m wind for the CNTL experiment and friction velocity for the STAT and DYN experiments) and show the anomaly of the cube of the wind speed, as it is the cube of the value that affects dust emission (equations (1) and (2)). For simplicity we only show soil wetness and bareness for the experiments for which those values are relevant and time varying. Figure 3 shows that while surface wind speed does vary throughout the El Niño event, it is not coherently related to dust emission, and the anomalies are particularly small during the peak of the El Niño event when dust emission anomalies are greatest. The changes to the land surface prove to be more influential than the changes in wind speed. Soil wetness is anomalously low throughout the El Niño, tracking the precipitation anomalies with a slight lag. Reduced soil wetness more often stays below the threshold to cut off dust emission, allowing the new parameterization to emit dust more frequently during these dry periods. Additionally, the vegetation dieback that occurs in the DYN experiment due to diminished soil water increases the bareness of the land tiles. The 6–8% increase in bareness shown in Figure 3 accounts for approximately half of the overall increase in dust emission for the DYN experiment. It is also noteworthy that the bareness anomalies lag the precipitation and soil wetness anomalies by several months, providing a mechanism for sustaining enhanced dust emission beyond the period of anomalous dry periods.

4. Discussion

We have presented here what are, to the best of our knowledge, the first multicentury, unconstrained GCM simulations to produce large decadal variability of dust emission from Australia. Inclusion of dynamic soil moisture and vegetation amplifies the dust emission variability in the GFDL CM3 model and captures the DOD-ENSO relationship. Central Australia is an especially apt location to experience such amplification, as it experiences large changes in precipitation and concomitant changes in vegetation. It is possible that less amplification would occur in other dust-emitting regions, such as the Sahara, where wet soil and vegetation are rarely sustained even in the relatively wet years. In Australia, where these variables respond strongly to ENSO events, including the land surface information in dust emission calculations is crucial to simulating both

the observed long-term variability and the ENSO-dust relationship. Indeed, during El Niño events, land surface anomalies are more important to dust emission than meteorological anomalies.

Enhanced dust variability has important implications for regional climate in and around Australia. As a primarily scattering aerosol, dust is responsible for a negative radiative forcing at the surface, while its effect at the top of atmosphere (TOA) depends on the relative reflectivity of the airborne dust and the surface below. Generally speaking, dust is more reflective than the surface, creating a cooling effect at TOA. Figure 4 shows how aerosol radiative forcing over Australia responds to El Niño in the control and dynamic vegetation runs. At the surface, the slight dust enhancement in the control run (Figure 2) yields up to $-15\ W/m^2$ forcing, compared to more than $-20\ W/m^2$ in the dynamic vegetation run. At TOA the control run actually experiences a positive radiative forcing near the equator, which is explained by increased absorption by black carbon overwhelming increased scattering by dust, as black carbon lifetimes increase when precipitation declines during El Niño. In the DYN experiment, the scattering dust creates a TOA radiative forcing greater than $-1\ W/m^2$ per unit of the Nino3.4 index. The shape of the radiative forcing pattern is that of the dust plume, with pronounced minima where the plume passes over regions of lower surface albedo such as the ocean, eastern forests, and darker parts of the northwestern deserts. The strongly negative surface radiative forcing is expected to cool the surface and reduce sensible and latent heat fluxes [*Ramanathan et al.*, 2001]. This in turn implies a more stable lower atmosphere that may provide a pathway for dust to suppress rainfall over much of Australia and create a dust-drought positive feedback. The presence of such a feedback has been discussed in the literature regarding other locations [e.g., *Cook et al.*, 2012] and may explain the slightly stronger precipitation response to ENSO in the STAT and DYN experiments (Figure 2). *Rotstayn et al.* [2011] found that Australian dust enhanced ENSO-related rainfall anomalies, though their analysis attributed the effect to moisture advection rather than atmospheric stability. Lastly, we note that enhanced dust variability from Australia implies greater variability in dust deposition over much of the Southern Hemisphere, with subsequent impacts on ocean productivity and paleoclimate records.

Acknowledgments

We are grateful to John Dunne and John Wilson for providing helpful commentary on the manuscript and Niki Zadeh and Larry Horowitz for modeling assistance. The MODIS Deep Blue aerosol product was acquired from the Level 1 and Atmosphere Archive and Distribution System (LAADS) Distributed Active Archive Center (DAAC), while the GPCP data were acquired from Mesoscale Atmospheric Processes Group, both located in the Goddard Space Flight Center in Greenbelt, MD. The data products associated with this paper can be obtained by contacting first author Stuart Evans. This research has been funded by the Princeton Environmental Institute at Princeton University through the Carbon Mitigation Initiative.

References

Adler, R. F., et al. (2003), The version 2 Global Precipitation Climatology Project (GPCP) monthly precipitation analysis (1979–present), *J. Hydrometeor.*, *4*, 1147–1167.

Anderson, T. L., Y. Wu, D. A. Chu, B. Schmid, J. Redemann, and O. Dubovik (2005), Testing the MODIS satellite retrieval of aerosol fine-mode fraction, *J. Geophys. Res.*, *110*, D18204, doi:10.1029/2005JD005978.

Balkanski, Y., M. Schulz, T. Claquin, and S. Guibert (2007), Reevaluation of mineral aerosol radiative forcings suggests a better agreement with satellite and AERONET data, *Atmos. Chem. Phys.*, *7*, 81–95, doi:10.5194/acp-7-81-2007.

Boyd, P. W., G. McTainsh, V. Sherlock, K. Richardson, S. Nichol, M. Ellwood, and R. Frew (2004), Episodic enhancement of phytoplankton stocks in New Zealand subantarctic waters: Contribution of atmospheric and oceanic iron supply, *Global Biogeochem. Cycles*, *18*, GB1029, doi:10.1029/2002GB002020.

Chan, Y.-C., G. McTainsh, J. Leys, H. McGowan, and K. Tews (2005), Influence of the 23 October 2003 dust storm on the air quality of four Australian cities, *Water Air Soil Pollut.*, *164*, 329–348, doi:10.1007/s11270-005-4009-0.

Cook, B. I., R. L. Miller, and R. Seager (2009), Amplification of the North American "Dust Bowl" drought through human-induced land degradation, *Proc. Nat. Acad. Sci.*, *106*, 4997–5001, doi:10.1073/pnas.0810200106.

Cook, B. I., R. Seager, R. L. Miller, and J. A. Mason (2012), Intensification of North American megadroughts through surface and dust aerosol forcing, *J. Clim.*, *26*, 4414–4430, doi:10.1175/JCLI-D-12-00022.1.

Donner, L. J., et al. (2011), The dynamical core, physical parameterizations, and basic simulation characteristics of the atmospheric component AM3 of the GFDL global coupled model CM3, *J. Climate*, *24*, 3484–3519, doi:10.1175/2011JCLI3955.1.

Evan, A. T., C. Flamant, S. Fiedler, and O. Doherty (2014), An analysis of aeolian dust in climate models, *Geophys. Res. Lett.*, *41*, 5996–6001, doi:10.1002/2014GL060545.

Evans, S. M., R. Marchand, and T. P. Ackerman (2014), Variability of the Australian monsoon and precipitation trends at Darwin, *J. Climate*, *27*, 8487–8500, doi:10.1175/JCLI-D-13-00422.1.

Gabric, A. J., R. A. Cropp, G. H. McTainsh, B. M. Johnston, H. Butler, B. Tilbrook, and M. Keywood (2010), Australian dust storms in 2002–2003 and their impact on Southern Ocean biogeochemistry, *Global Biogeochem. Cycles*, *24*, GB2005, doi:10.1029/2009GB003541.

Ginoux, P., M. Chin, I. Tegen, J. M. Prospero, B. Holben, O. Dubovik, and S.-J. Lin (2001), Sources and distributions of dust aerosols simulated with the GOCART model, *J. Geophys. Res.*, *106*, 20,255–20,273, doi:10.1029/2000JD000053.

Ginoux, P., J. M. Prospero, T. E. Gill, N. C. Hsu, and M. Zhao (2012), Global-scale attribution of anthropogenic and natural dust sources and their emission rates based on MODIS Deep Blue aerosol products, *Rev. Geophys.*, *50*, RG3005, doi:10.1029/2012RG000388.

Goudie, A. S., and N. J. Middleton (1992), The changing frequency of dust storms through time, *Clim. Change*, *20*, 197–225.

Hsu, N. C., M.-J. Jeong, C. Bettenhausen, A. M. Sayer, R. Hansell, C. S. Seftor, J. Huang, and S.-C. Tsay (2013), Enhanced Deep Blue aerosol retrieval algorithm: The second generation, *J. Geophys. Res. Atmos.*, *118*, 9296–9315, doi:10.1002/jgrd50712.

Huffman, G. J., R. F. Adler, D. T. Bolvin, and G. Gu (2009), Improving the global precipitation record: GPCP Version 2.1, *Geophys. Res. Lett.*, *36*, L17808, doi:10.1029/2009GL040000.

Hurtt, G. C., et al. (2011), Harmonization of land-use scenarios for the period 1500–2100: 600 years of global gridded annual land-use transitions, wood harvest, and resulting secondary lands, *Clim. Change*, *109*, 117–161, doi:10.1007/s10584-011-0153-2.

Leys, J., G. McTainsh, C. Strong, S. Heidenreich, and K. Biesaga (2008), DustWatch: Using community networks to improve wind erosion monitoring in Australia, *Earth Surf. Process. Landforms*, *33*, 1912–1926, doi:10.1002/esp.1733.

Leys, J. F., S. K. Heideneich, C. L. Strong, G. H. McTainsh, and S. Quigley (2011), PM 10 concentrations and mass transport during "Red Dawn"—Sydney 23 September 2009, *Aeolian Res.*, *3*, 327–342.

Lotsch, A., M. A. Friedl, and B. T. Anderson (2003), Coupled vegetation-precipitation variability observed from satellite and climate records, *Geophys. Res. Lett.*, *30*, 1774, doi:10.1029/2003GL017506.

Mahowald, N. M., et al. (2010), Observed 20th century desert dust variability: Impact on climate and biogeochemistry, *Atmos. Chem. Phys.*, *10*, 10,875–10,893, doi:10.5194/acp-10-10875-2010.

Marx, S. K., H. A. McGowan, and B. S. Kamber (2009), Long-range dust transport from eastern Australia: A proxy for Holocene aridity and ENSO-type climate variability, *Earth Planet. Sci. Lett.*, *282*, 167–177, doi:10.1016/j.epsl.2009.03.013.

Milly, P. C. D., S. Malyshev, E. Shevliakova, K. A. Dunne, K. L. Findell, T. Gleeson, Z. Lianh, P. Phillipps, R. J. Stouffer, and S. Swenson (2014), An enhanced model of land water and energy for global hydrologic and earth-system studies, *J. Hydrometeorology*, *15*, 1739–1761, doi:10.1175/JHM-D-13-0162.1.

Prospero, J. M., P. Ginoux, O. Torres, S. E. Nicholson, and T. E. Gill (2002), Environmental characterization of global sources of atmospheric soil dust identified with the Nimbus 7 Total Ozone Mapping Spectrometer (TOMS) absorbing aerosol product, *Rev. Geophys.*, *40*(1), 1002, doi:10.1029/2000RG000095.

Ramanathan, V., P. J. Crutzen, J. T. Kiehl, and D. Rosenfeld (2001), Aerosols, climate, and the hydrological cycle, *Science*, *294*, 2119–2124.

Revel-Rolland, M., P. De Deckker, B. Delmonte, P. P. Hesse, J. W. Magee, I. Basile-Doelsch, F. Grousset, and D. Bosch (2006), Eastern Australia: A possible source of dust in East Antarctica interglacial ice, *Earth and Plan. Sci. Let.*, *249*, 1–13, doi:10.1016/j.epsl2006.06.028.

Risbey, J. R., M. J. Pook, P. C. McIntosh, M. C. Wheeler, and H. H. Hendon (2009), On the remote drivers of rainfall variability in Australia, *Mon. Weather Rev.*, *137*, 3233–3253, doi:10.1175/2009MWR2861.1.

Rotstayn, L. D., M. A. Collier, R. M. Mitchell, Y. Qin, K. Campbell, and S. M. Dravitski (2011), Simulated enhancement of ENSO-related rainfall variability due to Australian dust, *Atmos. Chem. Phys.*, *11*, 6575–6592, doi:10.5194/acp-11-6575-2011.

Sayer, A. M., N. C. Hsu, C. Bettenhausen, and M.-J. Jeong (2013), Validation and uncertainty estimates for MODIS Collection 6 "Deep Blue" aerosol data, *J. Geophys. Res. Atmos.*, *118*, 7864–7873, doi:10.1002/jgrd.50600.

Shao, Y., and L. M. Leslie (1997), Wind erosion prediction over the Australian continent, *J. Geophys. Res.*, *102*, 30,091–30,105, doi:10.1029/97JD02298.

Shao, Y., K.-H. Wyrwoll, A. Chappell, J. Huang, Z. Lin, G. H. McTainsh, M. Mikami, T. Y. Tanaka, X. Wang, and S. Yoon (2011), Dust cycle: An emerging core theme in Earth system science, *Aeolian Res.*, *2*, 181–204, doi:10.1016/j.aeolia.2011.02.001.

Shevliakova, E., S. W. Pacala, S. Malyshev, G. C. Hurtt, P. C. D. Milly, J. P. Casperson, L. T. Sentman, J. P. Fisk, C. Wirth, and C. Crevoisier (2009), Carbon cycling under 300 years of land use change: Importance of the secondary vegetation sink, *Global Biogeochem. Cycles*, *23*, GB2022, doi:10.1029/2007GB003176.

Stanelle, T., I. Bey, T. Raddatz, C. Reick, and I. Tegen (2014), Anthropogenically induced changes in twentieth century mineral dust burden and the associated impact on radiative forcing, *J. Geophys. Res. Atmos.*, *119*, 13,526–13,546, doi:10.1002/2014JD022062.

Strong, C. L., K. Parsons, G. H. McTainsh, and A. Sheehan (2010), Dust transporting wind systems in the lower Lake Eyre Basin, Australia: A preliminary study, *Aeolian Res.*, *2*, 205–214, doi:10.1016/j.aeolia.2010.11.001.

Volz, F. E. (1973), Infrared optical constants of ammonium sulfate, Sahara dust, volcanic pumice, and flyash, *Appl. Optics*, *12*, 564–568.

Wang, B., and Q. Ding (2008), Global monsoon: Dominant mode of annual variation in the tropics, *Dyn. Atmos. Oceans*, *44*, 165–183, doi:10.1016/j.dynatmoce.2007.05.002.

Zender, C. S., and E. Y. Kwon (2005), Regional contrasts in dust emission responses to climate, *J. Geophys. Res.*, *110*, D13201, doi:10.1029/2004JD005501.